Low-lying dipole response in the Relativistic Quasiparticle Time Blocking Approximation and its influence on neutron capture cross sections

E. Litvinova [a,b,c], H. P. Loens [a,d], K. Langanke [a,c,d], G. Martínez-Pinedo [a], T. Rauscher [e], P. Ring [f], F.-K. Thielemann [e] and V. Tselyaev [g]

[a] *GSI Helmholtzzentrum für Schwerionenforschung, Planckstr. 1, 64291 Darmstadt, Germany*

[b] *Institute of Physics and Power Engineering, Pl. Bondarenko1, 249033 Obninsk, Russia*

[c] *Frankfurt Institute for Advanced Studies, Ruth-Moufang Str. 1, 60438 Frankfurt, Germany*

[d] *Technische Univeristät Darmstadt, Institut für Kernphysik, Schlossgartenstr. 9, 64289 Darmstadt, Germany*

[e] *Department of Physics, University of Basel, Klingelbergstr. 82, 4056 Basel, Switzerland*

[f] *Physik-Department, Technische Universität München, 85748 Garching, Germany*

[g] *Nuclear Physics Department, V. A. Fock Institute of Physics, St. Petersburg State University, 198504 St. Petersburg, Russia*

arXiv:0903.5439v1 [nucl-th] 31 Mar 2009

Abstract

We have computed dipole strength distributions for nickel and tin isotopes within the Relativistic Quasiparticle Time Blocking approximation (RQTBA). These calculations provide a good description of data, including the neutron-rich tin isotopes ^{130,132}Sn. The resulting dipole strengths have been implemented in Hauser-Feshbach calculations of astrophysical neutron capture rates relevant for r-process nucleosynthesis studies. The RQTBA calculations show the presence of enhanced dipole strength at energies around the neutron threshold for neutron rich nuclei. The computed neutron capture rates are sensitive to the fine structure of the low lying dipole strength, which emphasizes the importance of a reliable knowledge of this excitation mode.

Key words: relativistic many-body theory, Hauser-Feshbach theory, neutron capture, astrophysical reaction rates, r-process

1 Introduction and motivation

Neutron capture cross sections are one of the essential nuclear inputs for studies of r-process nucleosynthesis. As this astrophysical process, which produces about half of the heavy elements in the universe, runs through nuclei with extreme neutron excesses, most of the needed cross sections are not experimentally known and have to be modelled. Such estimates are usually done on the basis of the statistical Hauser-Feshbach [1,2,3,4] model and require, as one of the important ingredients, the modelling of the electromagnetic transition strength from nuclear states above the neutron threshold. Often dipole transitions contribute dominantly to the cross sections. In the absence of experimental data, these dipole strength distributions for neutron-rich nuclei have been conventionally described by Lorentzians with an energy- or temperature-dependent width [5,6,7] and parameters derived from data for stable nuclei. Obviously deviations from the parametrized Lorentzian at energies around the neutron threshold can lead to significant modifications of the neutron capture cross sections. As noted first by Goriely [8], such effects can arise from the so-called pygmy resonance which leads to an enhancement of the low-lying E1 strength, potentially in the astrophysically important energy range. In fact, an enhancement of the E1 strength at excitation energies E_x below 10 MeV has been experimentally observed for neutron-rich nuclei relative to the one for stable nuclei. Prominent examples are the tin isotopes where the neutron-rich nuclei $^{129-132}$Sn exhibit a noticeable portion of the total E1 strength at $E_x < 10$ MeV, in contrast to the stable isotopes ^{116,120}Sn [9]. Theoretically these tendencies are well reproduced by calculations based on the Quasiparticle Random Phase Approximation (QRPA) on top of the Hartree-Fock plus Bardeen-Cooper-Schrieffer (HF-BCS) [10] or of the Hartree-Fock-Bogoliubov (HFB) [11] approaches and by the relativistic QRPA (RQRPA) calculations [12] and are usually explained as so-called pygmy resonances in which the excess neutrons oscillate against the isospin-saturated core. Significant progress has been achieved very recently by extending the RQRPA by the quasiparticle-phonon coupling model using the Relativistic Quasiparticle Time Blocking Approximation (RQTBA). As it has been demonstrated in [13], this extended approach reproduces the experimental E1 strength distributions in general very well, inluding the observed low-lying strength It has been also found that isotopic dependence of the excitation energy and the integrated strength of the pygmy dipole resonance agrees well with previous theoretical studies [14,15]. Ref. [16] has shown that once the theoretical strength distributions are corrected for the experimental detector response and in particular for the fact that Coulomb dissociation experiments can only access strength above

the neutron threshold, the data for ^{130}Sn and ^{132}Sn [17] are nicely reproduced. This motivates us to use this model to calculate the E1 strength distributions for the chains of tin and nickel isotopes, including nuclei close and on the r-process path for which data do not exist, yet. The focus of our studies is on the effect of enhanced low-lying dipole strength on neutron capture cross sections, in particular for neutron-rich nuclei. Our calculations are based on the statistical model which we briefly describe in the next section. In section 3 we present the RQTBA dipole strength functions and compare them with standard Lorentzian parametrizations [3] and with the QRPA calculations of Ref. [10]. The impact of different dipole strength distributions on neutron-capture rates for the nickel and tin isotopes is also discussed.

2 Formalism

The Hauser-Feshbach expression for the cross section of an (n, γ) reaction proceeding from the target nucleus i in the state μ with spin J_i^μ and parity π_i^μ to a final state ν with spin J_m^ν and parity π_m^ν in the residual nucleus m via a compound state with excitation energy E, spin J, and parity π is given by (see also [2,3,18])

$$\sigma_{(n,\gamma)}^{\mu\nu}(E_{i,n}) = \frac{\pi\hbar^2}{2M_{i,n}E_{i,n}} \frac{1}{(2J_i^\mu + 1)(2J_n + 1)} \sum_{J,\pi} (2J+1) \frac{T_n^\mu T_\gamma^\nu}{T_{\text{tot}}}, \qquad (1)$$

where $E_{i,n}$ and $M_{i,n}$ are the center-of-mass energy and the reduced mass for the initial system. $J_n = 1/2$ is the neutron spin. For (n, γ) reactions the residual and the compound nucleus are the same. The transmission coefficients $T_n^\mu = T_n(E, J, \pi; E_i^\mu, J_i^\mu, \pi_i^\mu)$, $T_\gamma^\nu = T_\gamma(E, J, \pi; E_m^\nu, J_m^\nu, \pi_m^\nu)$ describe the transitions from the compound state - characterized by (E, J, π) - to the initial and final state, respectively. The sum of the transmission coefficients over all possible exit-channels is given by T_{tot}. It is possible to derive the laboratory cross section (the target is in its ground state, e.g. $\mu = 0$) from Eq. (1) by summing over all possible final states ν in the residual nucleus. Therefore it is convenient to introduce transmission coefficients which only depend on the compound quantum numbers:

$$T_\gamma(E, J, \pi) = \sum_\nu T_\gamma(E, J, \pi; E_m^\nu, J_m^\nu, \pi_m^\nu). \qquad (2)$$

Generally the discrete energy spectrum is only partially known and consequently above a certain excitation energy a level density description is applied. In that case the sum in Eq. (2) translates into a discrete sum plus an integration over the level density [2,3,18]:

$$T_\gamma(E, J, \pi) = \sum_{\nu=0}^{\kappa} T_\gamma(E, J, \pi; E_m^\nu, J_m^\nu, \pi_m^\nu) \tag{3}$$

$$+ \int_{E_m^\kappa}^{E} \sum_{J_m, \pi_m} T_\gamma(E, J, \pi; E_m, J_m, \pi_m) \rho(E_m, J_m, \pi_m) dE_m.$$

where E_m^κ is the excitation energy of the last experimentally known state, κ, in the nucleus m.

In the calculation of the transmission coefficient we closely follow the formalism as described in [3,19]. In particular we consider parity-dependent level densities for initial, compound and final states, here following [20]. The parity-dependent level densities were taken from Hilaire and Goriely as calculated within a combinatorial approach on top of HFB single particle energies [21]. We note that using a standard backshifted Fermi gas level density [4,3] with a parity-dependence as introduced in [22] gives quite similar results.

The γ-transmission coefficient for the decay to a state ν involves a sum over all possible photon multipolarities. For a given multipolarity, XL, and photon energy $E_\gamma = E - E^\nu$, the transmission coefficient is related with the γ-strength function, f_{XL}, via

$$T_{XL}(E, J, \pi, E^\nu, J^\nu, \pi^\nu) = T_{XL}(E, E_\gamma) = 2\pi E_\gamma^{2L+1} f_{XL}(E, E_\gamma). \tag{4}$$

In this paper we mainly focus on E1 transitions, although the M1 contributions have been calculated as well using the single-particle approach [2,23]. Both multipolarities usually dominate for neutron capture reactions at astrophysical energies.

In general, the strength function depends on the initial and final states. However, in practical applications, one usually adopts the Brink-Axel hypothesis which assumes that the strength function is independent of the detailed structure of the initial state and consequently depends only on E_γ and not on E [24,25,26]. Assuming that the photoabsorption process does not depend on the spin of the final state, it is possible to relate the cross section, σ_{XL}, to the γ-strength function:

$$f_{XL}(E, E_\gamma) = f_{XL}(E_\gamma) = \frac{1}{2L+1} \frac{\sigma_{XL}(E_\gamma)}{(\pi\hbar c)^2} \cdot E_\gamma^{-2L+1}. \tag{5}$$

According to Eq. (5), the γ-strength function and the absorption cross section for E1 transitions are connected via

$$\sigma_{E1}(E_\gamma) = 3\pi^2 (\hbar c)^2 E_\gamma f_{E1}(E_\gamma). \tag{6}$$

4

In statistical model calculations one usually assumes that the E1 strength distribution can be approximated by a Lorentzian adjusted to reproduce the position and width of the giant dipole resonance (GDR) [2,19,3,6,7]:

$$f_{\mathrm{E1}}(E_\gamma) = \frac{4}{3\pi} \frac{e^2}{\hbar c} \frac{1}{mc^2} \frac{NZ}{A} \frac{\Gamma E_\gamma}{(E_{\mathrm{E1}}^2 - E_\gamma^2)^2 + (E_\gamma \Gamma)^2}(1+\chi) \tag{7}$$

with N, Z and $A = N + Z$ being the neutron, proton and nucleon numbers of the compound nucleus. Here $\chi \approx 0.2$ is a factor that accounts for the neutron-proton exchange contribution (see e.g., [27]). The parameters E_{E1} and Γ are obtained by adjustment to data for the giant dipole resonance (see e.g., [28]) or, if data are not available, from theoretical model predictions or systematics [3]. The Lorentzian approach is known to be inaccurate in the low-energy region as the low energy tail of the Lorentzian usually overestimates the strength at these energies. In practical applications one therefore modifies the width of the GDR, Γ, to account for these deficiencies. Various treatments have been developed over the past decades (for an overview see [6] and references therein). Here we follow [5] and define an energy-dependent width parameter as: $\Gamma(E_\gamma) = \Gamma\sqrt{E_\gamma/E_{\mathrm{E1}}}$.

We have calculated RQTBA E1 strength functions as outlined in [13] and used them in combination with Eqs. (4,6) to obtain transmission coefficients for the E1 transitions. In the RQTBA, excitations in even-even nuclei are determined by the nuclear response function $R(\omega)$ whose matrix elements obey the Bethe-Salpeter equation (BSE) of the following form [13]:

$$\begin{aligned}
R_{k_1 k_4, k_2 k_3}^{\eta\eta'}(\omega) = {} & \tilde{R}_{k_1 k_2}^{(0)\eta}(\omega)\delta_{k_1 k_3}\delta_{k_2 k_4}\delta_{\eta\eta'} \\
& + \tilde{R}_{k_1 k_2}^{(0)\eta}(\omega) \sum_{k_5 k_6} \sum_{\eta''} \bar{W}_{k_1 k_6, k_2 k_5}^{\eta\eta''}(\omega) R_{k_5 k_4, k_6 k_3}^{\eta''\eta'}(\omega),
\end{aligned} \tag{8}$$

where indices k_i run over single-particle quantum numbers including states in the Dirac sea and indices η, η', η'' numerate forward (+) and backward (−) components in the quasiparticle space. Pairing correlations are treated in the BCS approximation. The quantity $\tilde{R}^{(0)}(\omega)$ describes free propagation of two quasiparticles in the mean field and matrix elements of the amplitude $\bar{W}$ read:

$$\bar{W}_{k_1 k_4, k_2 k_3}^{\eta\eta'}(\omega) = \tilde{V}_{k_1 k_4, k_2 k_3}^{\eta\eta'} + \left(\Phi_{k_1 k_4, k_2 k_3}^{\eta}(\omega) - \Phi_{k_1 k_4, k_2 k_3}^{\eta}(0) \right)\delta_{\eta\eta'}. \tag{9}$$

In Eq. (9) $\tilde{V}$ is the static part of the amplitude $\bar{W}$ based on a one-meson exchange interaction with a non-linear self-coupling between the mesons and determined by the relativistic energy functional with the parameter set NL3 [29]. $\Phi(\omega)$ is the dynamical part of the interaction amplitude responsible for

5

the particle-phonon coupling. It has been calculated in the quasiparticle time blocking approximation, see [13] for details.

To describe the observed spectrum of an excited nucleus in a weak external electromagnetic field P, one needs to calculate the strength function which is a convolution of the response function of Eq. (8) with matrix elements of the external field operator $P^{\eta}_{k_1 k_2}$:

$$S(E_\gamma) = -\frac{1}{2\pi} \lim_{\Delta \to +0} Im \sum_{k_1 k_2 k_3 k_4} \sum_{\eta \eta'} P^{\eta *}_{k_1 k_2} R^{\eta \eta'}_{k_1 k_4, k_2 k_3}(E_\gamma + i\Delta) P^{\eta'}_{k_3 k_4}. \qquad (10)$$

In the calculations a small finite imaginary part Δ of the energy variable is introduced for convenience in order to obtain a more smoothed envelope of the spectrum. This parameter has the meaning of an additional artificial width for each excitation. This width emulates effectively contributions from configurations which are not taken into account explicitly in our approach.

The dipole photo-absorption cross section,

$$\sigma_{E1}(E_\gamma) = \frac{16\pi^3 e^2}{9\hbar c} E_\gamma S_{E1}(E_\gamma), \qquad (11)$$

is expressed through the microscopically computed strength function of Eq. (10) and determines the dipole γ-strength function of Eq. (6) which is used for the statistical model calculations.

3   Results

We have calculated statistical model cross sections for (n, γ) reactions on tin and nickel isotopes using four different models to describe the dipole strength function. Our default model (model A) is the RQTBA which, as demonstrated in [13], reproduces experimental photo absorption cross sections very well, including the low-energy cross sections, which is of special interest for the discussion here. To account effectively for the residual effect of higher configurations beyond RQTBA, a 200 keV imaginary part has been included in the energy variable of Eq. (10). As the model is currently restricted to even-even nuclei, we will in the following only discuss neutron capture cross sections for odd-A nickel and tin isotopes. Following Refs. [2,3,19] we describe the dipole strength by a Lorentzian form of Eq. (7) with the energy dependent width parameter as defined above. The centroid E_{E1} and total strength are adjusted to the RQTBA strength function (model B). Although the width parameter is taken from Ref. [30], it gives a good reproduction of the RQTBA strength function

6

in the GDR region. A comparison between models A and B allows to disentangle the influence of the low-energy strength on the neutron capture cross sections. Finally, we have performed calculations using the Lorentzian form of Eq. (7) but with the strength parameters determined as described in Ref. [3] (Model C) and calculations adopting the dipole strength functions of Ref. [10], which have been derived by a QRPA approach on top of a Hartree-Fock-BCS model (model D).
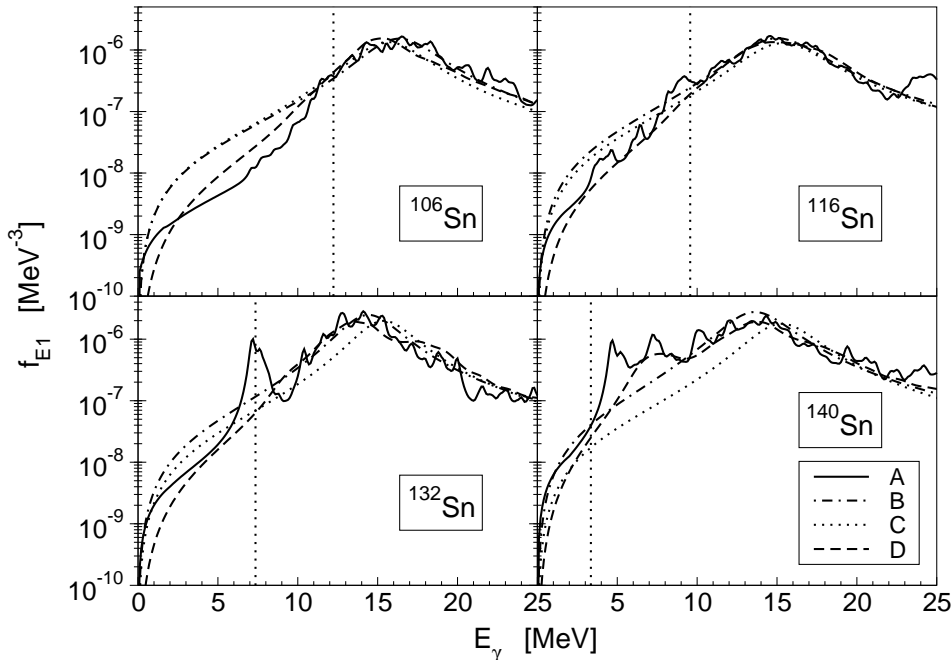

Fig. 1. γ strength functions for selected tin isotopes as calculated by the RQTBA approach (solid; model A) [13] and the QRPA model of Goriely and Khan [10] (dashed; model D). The dotted curves show the Lorentzian parametrization of the strength as proposed in [3] (model C) and the dash-dotted curves correspond to a Lorentzian with the width taken from [3], the centroid taken from the RQTBA results and the total strength adjusted to the RQTBA results, as explained in the text (model B). The dotted vertical lines indicate the (experimental) neutron threshold energies.

Fig. 1 shows the dipole γ strength functions for the four different models and selected tin isotopes. We note that models A and D reproduce the known photoabsorption cross section data for tin isotopes quite well [13,16]. While the parametrized strength function of Ref. [3] agrees nicely with the microscopic ^{116}Sn strength functions, it predicts a centroid energy which is somewhat higher for the neutron-rich tin isotope ^{132}Sn than obtained in the other models.

Comparing the various model predictions it is most striking that the microscopic model predicts quite noticeable nuclear structure effects which result in a rather strong fragmentation of the strength function. This is mainly due

to the quasiparticle-phonon coupling explicitly considered in the RQTBA approach [13]. Comparing the microscopic strength functions (model A) with the Lorentzian approximation of model B, we note that for most nuclei the parametrization overestimates the microscopic strength function at low energies, say $E < 5$ MeV. This indicates that the empirical energy-dependence of the width parameter [5] is not supported by the microscopic model. This conclusion is also supported by the QRPA results which are generally slightly smaller than the RQTBA results at the lowest energies. The standard parametrization utilized in [3] agrees quite well with the model B parametrization. However, with increasing neutron excess this model predicts the centroid at higher energies than the other models. Consequently, the γ strength function for ^{140}Sn in model C is smaller at low energies than in the other models.

As the RQTBA model includes phonon couplings which are absent in the QRPA model it resolves more nuclear structure details. This can lead to fluctuations in the γ strength function around the neutron threshold and below. An example is given by the nucleus ^{116}Sn (see Fig. 1) where the RQTBA model predicts a mild enhancement of the strength just at the neutron threshold which is absent in the QRPA model and, of course, in the parametrizations of models B and C. As the neutron separation energies move to lower energies with increasing neutron excess within a chain of isotopes, low-lying E1 strength as observed experimentally for the tin isotopes ^{130,132}Sn and found within our microscopic RQTBA approach for neutron-rich nuclei can influence the γ strength function around the neutron threshold significantly. A prominent example is ^{132}Sn where the RQTBA approach predicts a strong enhancement of the E1 strength around the neutron separation energy of $E = 7.3$ MeV. Such an increased strength is not predicted by the other models used in this paper (the relativistic QRPA calculations of Ref. [12] predict also additional strength at low energies) and, as we will see below, has a noticeable effect on the neutron capture cross sections. For ^{140}Sn the RQTBA model also predicts a strong fragmentation of the γ strength at low energies $E \gtrsim 5$ MeV with enhanced strength compared to the strengths of the other models. However, for this nucleus the neutron threshold is already quite low ($E_{\text{th}} = 3.5$ MeV) and this enhancement will only have modest effect on the cross sections.

By inserting the γ strength functions into Eqs. (1) and (4) we have calculated cross sections for neutron capture on the ground states of the isotopes ^{105,115,131,139}Sn arising solely from dipole transitions. The results are shown in Fig. 2 for neutron energies of up to 20 MeV (note that the maximum neutron energies reached in the r-process discussed below are of the order of $80 - 100$ keV). In order to understand the impact of various magnitudes of γ strengths it is necessary to realize what the relevant γ-ray energies are. It is well known that capture reactions proceeding via the compound reaction mechanism result in a γ-ray cascade with a dominant contribution coming from γ rays with only a few MeV, below the neutron separation energy S_n.
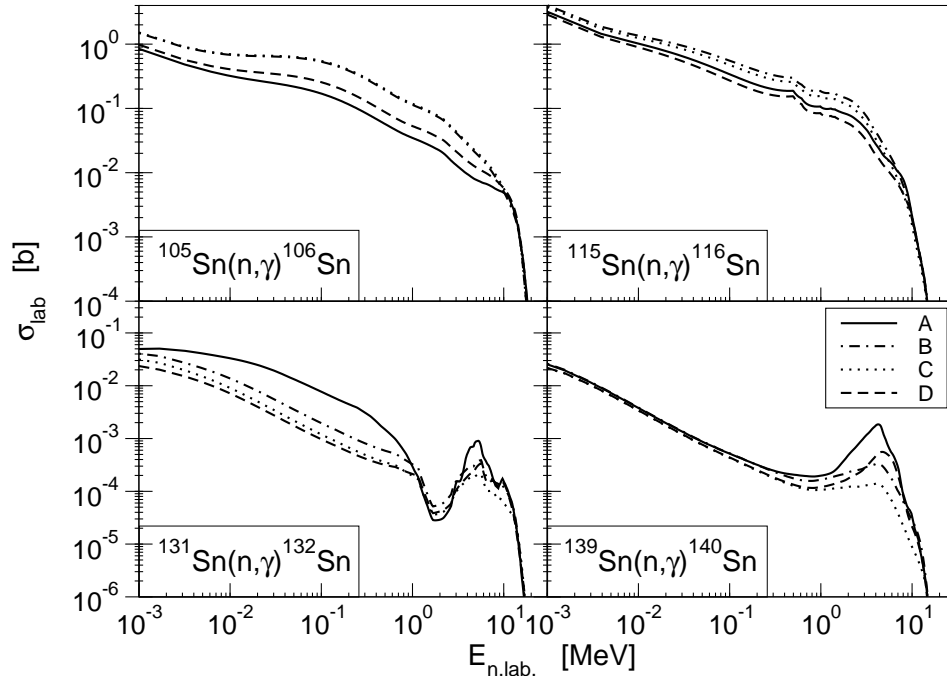
8

Fig. 2. Cross sections for (n, γ)-reactions on various tin isotopes based on E1 strength functions as derived in different models, see Fig. 1 and text.

Recently, Ref. [31], assuming the validity of the Brink-Axel hypothesis and a Lorentzian parametrization of the dipole strength, has shown that this also holds for neutron-rich targets with dominant E1 strength leading to levels at 3-4 MeV below S_n unless the density of levels accessible by E1 transition is low. In the latter case, γ transitions with the maximally possible energy of $S_n + E_n$ may dominate. This nicely explains the dependences we find in our calculations. For the cases of neutron captures on ^{105}Sn and ^{115}Sn the dominating γ transitions display an energy of $E_\gamma \approx 3 + E_n$ MeV with dominant E1 transition endpoints at ≈ 3 MeV below S_n. Scanning through E_n, we can nicely see in Figs. 1,2 how the larger strength functions of the two parametrized descriptions (models B and C) result in larger cross sections than those obtained with the microscopic approaches RQTBA and QRPA (models A and D), until the predictions converge close to S_n. The RQTBA model predicts a strong fragmentation of the dipole strength at low energies. However, this is not seen in the cross sections because the relevant range of available γ energies averages and smoothes the impact of the fluctuations. The small kink appearing in the ^{115}Sn cross section at $E_n = 0.5$ MeV is due to the opening of the (n, p) channel.

Consistent with [31], we find a different behavior in the cross sections of ^{131}Sn. The low level density of the doubly magic compound (and final) nucleus ^{132}Sn causes the dominance of γ transitions directly to the ground state, with $E_\gamma = S_n + E_n$. Up to $E_n < 1$ MeV the influence of the RQTBA pygmy peak explains why the RQTBA yields the by far largest cross sections up to that energy.

9

Above that energy, the RQTBA γ strength drops below the strengths predicted by the other models and consequently the resulting cross section becomes the smallest. After another $2 - 3$ MeV (note that Fig. 1 uses a linear and Fig. 2 a logarithmic energy scale), the RQTBA predicts a larger γ strength again and consequently its respective cross section becomes the largest again. Interestingly, a second effect is overlaid on top of the general strength function behavior and giving rise to the decrease in cross sections found for all models around 2 MeV neutron energy. The level density description [21] predicts a relatively low density of negative parity states at excitation energies around 9 MeV in ^{132}Sn. In consequence, magnetic dipole transitions to the low-lying positive parity states dominate (not shown in Fig. 2). This is an example for the importance of the complete inclusion of parity-dependent level densities.

Except for the parity effect, the behavior of the ^{139}Sn(n, γ) cross section can be explained similarly to the one of ^{131}Sn. The level density below S_n is very low for such a neutron-rich nucleus and therefore the relevant γ energies are $E_\gamma = S_n + E_n$. The strong pygmy peak predicted by the RQTBA is also clearly seen in the cross section. Smaller fluctuations are dampened and the general strong decrease in the cross section at the high energy end is typical for Hauser-Feshbach cross sections, as in the other reactions considered here. In addition, for ^{139}Sn we find that the M1 contribution to the capture cross section exceeds the dipole part at low neutron energies (say $E_n < 100$ keV). Thus, at these energies the total cross sections are less affected by the differences in the dipole strength functions. However, our statistical model code uses a rather simple description of M1 transitions based on a single particle treatment [2,23]. A more appropriate treatment, which includes the concentration of the M1 strength around $E = 7$–10 MeV due to spin excitations and in addition considers the pronounced orbital contribution seen in deformed nuclei (scissors mode [32]) is called for.

The classical r-process operates at a typical stellar temperature of order 10^9 K [3]. To estimate which impact the enhanced low-energy dipole strength could have on neutron capture rates under astrophysical conditions, we have calculated the stellar neutron capture rate $\langle \sigma v \rangle$, where σ is the neutron capture cross section, v is the relative velocity of the fusing nuclei in the initial channel and the symbol $\langle ... \rangle$ indicates proper averaging over the Maxwell-Boltzmann velocity distributions of the two nuclei at the stellar temperature and accounting for the thermal population of excited states. In Fig. 3 we compare ratios of neutron capture rates as obtained in the four different models at a temperature of $T = 10^9$ K. The capture rates have been computed neglecting M1 transitions due to their rather simple treatment in our statistical code (see paragraph above). We observe that rates calculated with the parametrized E1 strengths are usually larger than our RQTBA results with the noticeable exception for the isotopes ^{130,132}Sn (capturing the neutron on ^{129,131}Sn). With the additional observation that the other microscopically calculated strength functions
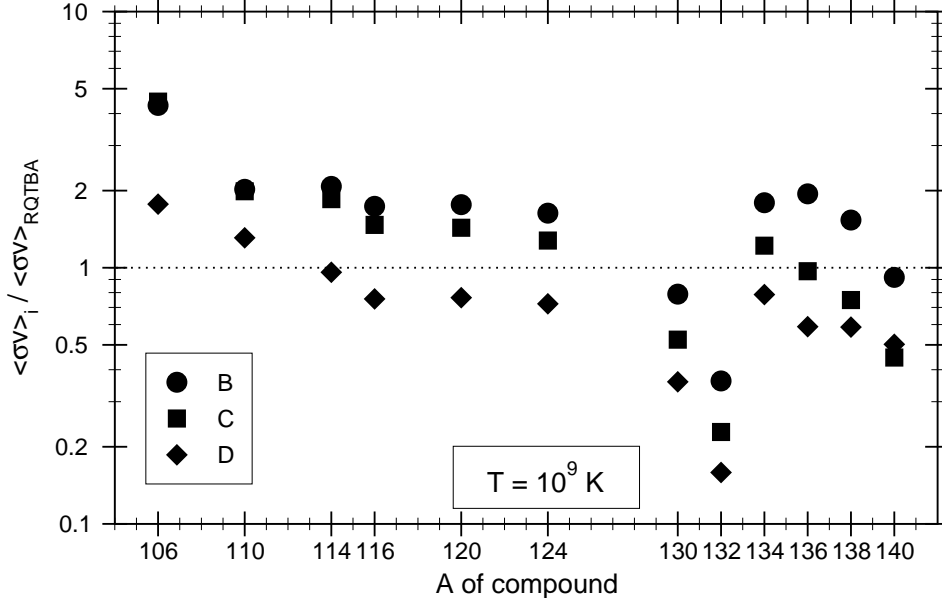
Fig. 3. Ratios of the stellar neutron capture rates at a temperature $T = 10^9$ K for tin isotopes as calculated within models B, C, and D relative to those obtained in model A (RQTBA). All the calculations consider only E1 gamma transitions. For descriptions of the models, see text.

(QRPA, model D) generally predicts smaller rates than the parametrization models one might conclude that the parametrization of the dipole strength functions with the energy dependence as defined above seems to predict too large strength at low gamma energies (except for the most neutron-rich tin isotope, ^{140}Sn, considered in this work) and hence overestimates the rates, compared to microscopic models. Interestingly, we do not observe by comparison of the four models that the low-lying strength is more important in neutron-rich nuclei as, for example, the parametrized strength of model B exceeds the RQTBA results by about the same amount in the neutron deficient and stable tin isotopes as it does in the very neutron-rich ones ($^{133-137}$Sn).

We have also performed calculations of dipole strength functions, cross sections and neutron capture rates at $T = 10^9$ K for the even neutron-rich nickel isotopes $^{68-78}$Ni. A comparison of the rates obtained in our four different models is shown in Fig. 4. The findings are quite similar to those for the tin isotopes. For all isotopes the rates calculated with the parametrized dipole strength (models B and C) exceeds those obtained on the basis of the RQTBA strength functions, again pointing to a non-adequate description of the low-lying strength by the energy dependent width parameter as chosen in [3]. Except for the capture on ^{67}Ni, the agreement between the two microscopic approaches (models A and D) is quite satisfactory. The Lorentzian parametrization slightly overestimates the microscopic rates. We note, however, that for the heaviest nickel nuclei the parametrization used within Ref. [3] predicts the centroid of the giant dipole resonance at slightly higher energies. If corrected, the downwards
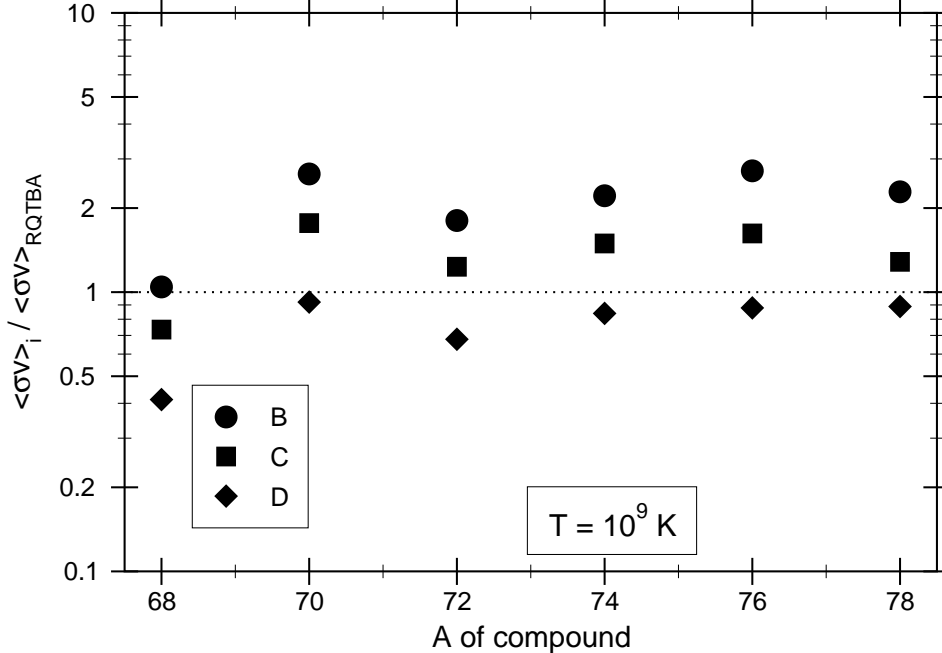
11

Fig. 4. Ratios of the stellar neutron capture rates at a temperature $T = 10^9$ K for nickel isotopes as calculated within models B, C, and D relative to those obtained in model A (RQTBA). All the calculations consider only E1 gamma transitions. For descriptions of the models, see text.

shift in energy would result in somewhat larger rates.

In general, our calculations for the capture rates on tin and nickel isotopes show a rather close agreement between the models suggesting that the enhanced low-lying dipole strength predicted by theoretical models and experimentally observed for selected nuclei has only modest influence on the neutron capture rates. The largest effect we find for the capture on the tin isotopes ^{129,131}Sn (caused by low-lying dipole strength in ^{130,132}Sn) where our microscopic RQTBA model predicts noticeable enhanced strength just around the energies of the neutron threshold, leading to an increase in the capture rate by factors 2–5 compared to the other models considered here.

The coincidence that the enhanced E1 strength lies around the neutron threshold in ^{132}Sn and a large portion of the transitions goes to the daughter ground state (due to suppression of excited states at modest excitation energies in this double-magic nucleus) results in a large enhancement of the reaction rate in the RQTBA model compared to the other models. As the RQTBA strength function for ^{132}Sn nicely agrees with data (see Fig. 1 of Ref. [16]), this change in the capture rate should be adopted in future r-process simulations.

4 Conclusions

We have obtained E1 strength functions for nickel and tin isotopes based on the microscopic RQTBA approach which has been proven previously to give a good description of data, including those for the neutron-rich tin isotopes ^{130,132}Sn. These data show E1 strengths at energies around the neutron threshold which are enhanced compared to the expectations from a Lorentzian parametrization of the giant resonance. As it has been pointed out before that such enhanced dipole strengths could have noticeable effects on neutron capture rates for r-process nuclei, we have calculated the respective capture cross sections for the relevant nickel and tin isotopes ($^{67-77}$Ni and $^{129-139}$Sn) and have compared the RQTBA results with rates obtained either within the non-relativistic QRPA on the basis of Hartree-Fock plus BCS calculations or by empirical parametrizations. Usually we find rather good agreement between the two microscopic models. Noticeable exceptions are ^{129,131}Sn, and in particular the capture rates to ^{132}Sn are noticeably larger within the RQTBA model than in all other models, which is caused by the enhanced dipole strength in this nucleus at energies above the neutron threshold. We note, however, that our calculation of the capture rates are based on the Brink-Axel hypothesis, which is common in statistical model evaluations of neutron capture rates for r-process applications. Within this hypothesis an enhanced dipole strength around the neutron threshold translates to enhanced neutron capture cross sections only if transitions to the ground state dominate. If the capture leads to excited states instead the strength function at appropriate lower energies is relevant. However, the transition strength for excited states could be different than for the ground state at the moderate energies relevant to neutron capture, invalidating the Brink-Axel hypothesis. Consequently, tests of this hypothesis for dipole transitions, similar to those performed for Gamow-Teller transitions in Ref. [33] are welcome.

Two final remarks are in order. At first, the RQTBA model predicts fragmentation and low-lying strengths also in the neutron-rich isotopes, however, not at the low energies close to the neutron threshold. Whether further correlations beyond the RQTBA model will further push strength to lower energies and hence might enhance the dipole cross sections at low neutron energies is an open question and must wait until appropriate nuclear models can be applied to such nuclei. Secondly, we have also calculated the contributions of other multipoles to the neutron capture rate and find that for the tin isotopes beyond ^{132}Sn, which have quite low neutron thresholds, M1 transitions dominate in our calculations making the observed differences in the dipole cross sections unimportant for the total cross sections due to our use of parity-dependent level densities [20]. However, we note that our statistical model code describes M1 transitions in the so-called single-particle treatment. The calculation of the M1 transitions should generally be improved by using M1 strength functions

which resemble the experimentally observed energy distribution with strong spin contributions around excitation energies of order 7–10 MeV and orbital contributions at low energies, including the pronounced scissors mode [32] in deformed nuclei at excitation energies of $E \approx 2$–3 MeV, i.e. around neutron threshold energies in very neutron-rich nuclei.

Acknowledgements

References

[1] W. Hauser, H. Feshbach, Phys. Rev. **87** (1952) 366.

[2] J. A. Holmes, S. E. Woosley, W. A. Fowler, B. A. Zimmerman, At. Data Nucl. Data Tables **18** (1976) 305.

[3] J. J. Cowan, F.-K. Thielemann, J. W. Truran, Phys. Rep. **208** (1991) 267.

[4] T. Rauscher, F.-K. Thielemann, K.-L. Kratz, Phys. Rev. C **56** (1997) 1613.

[5] C. M. McCullagh, M. L. Stelts, R. E. Chrien, Phys. Rev. C **23** (1981) 1394.

[6] T. Belgya, *et al.*, *Handbook for calculations of nuclear reaction data, RIPL-2*, IAEA-TECDOC-1506 (IAEA, Vienna, 2006), available online at http://www-nds.iaea.org/RIPL-2/.

[7] J. Kopecky, M. Uhl, Phys. Rev. C **41** (1990) 1941.

[8] S. Goriely, Phys. Lett. B **436** (1998) 10.

[9] A. Klimkiewicz, *et al.* (LAND Collaboration), Phys. Rev. C **76** (2007) 051603.

[10] S. Goriely, E. Khan, Nucl. Phys. A **706** (2002) 217.

[11] S. Goriely, E. Khan, M. Samyn, Nucl. Phys. A **739** (2004) 331.

[12] N. Paar, P. Ring, T. Nikšić, D. Vretenar, Phys. Rev. C **67** (2003) 034312.

[13] E. Litvinova, P. Ring, V. Tselyaev, Phys. Rev. C **78** (2008) 014312.

[14] N. Paar, D. Vretenar, E. Khan, and G. Colò, Rep. Prog. Phys. **70** (2007) 691.

[15] N. Tsoneva and H. Lenske, Phys. Rev. C **77** (2008) 024321.

[16] E. Litvinova, P. Ring, V. Tselyaev, K. Langanke, `arXiv:0811.1423[nucl-th]`, to be published in Phys. Rev. C (2009).

[17] P. Adrich, *et al.* (LAND-FRS Collaboration), Phys. Rev. Lett. **95** (2005) 132501.

[18] T. Rauscher, F.-K. Thielemann, At. Data Nucl. Data Tables **75** (2000) 1.

[19] F.-K. Thielemann, M. Arnould, J. Truran, in *Advances in Nuclear Astrophysics*, edited by E. Vangioni-Flam, J. Audouze, M. Casse, J.-P. Chieze, J. Tran Thanh van (1987), pp. 525–540.

[20] H. Loens, K. Langanke, G. Martínez-Pinedo, T. Rauscher, F.-K. Thielemann, Physics Letters B **666** (2008) 395.

[21] S. Hilaire, S. Goriely, Nucl. Phys. A **779** (2006) 63.

[22] D. Mocelj, *et al.*, Phys. Rev. C **75** (2007) 045805.

[23] J. M. Blatt, V. F. Weisskopf, *Theoretical Nuclear Physics* (Springer-Verlag, 1952).

[24] G. A. Bartholomew, E. D. Earle, A. J. Ferguson, J. W. Knowles, M. A. Lone, Adv. Nucl. Phys. **7** (1973) 229.

[25] D. M. Brink, Ph.D. thesis, Oxford University (1955).

[26] P. Axel, in *Proceedings on International Symposium on Nuclear Structure* (IAEA Vienna, Dubna, 1968), p. 299.

[27] E. Lipparini, S. Stringari, Physics Reports **175** (1989) 103.

[28] S. S. Dietrich, B. L. Berman, At. Data Nucl. Data Tables **38** (1988) 199.

[29] G. A. Lalazissis, J. König, P. Ring, Phys. Rev. C **55** (1997) 540.

[30] F.-K. Thielemann, M. Arnould, in *Proc. Inter. Conf. on Nuclear Data for Science and Technology*, edited by K. Böckhoff (1983), p. 762.

[31] T. Rauscher, Phys. Rev. C **78** (2008) 032801(R).

[32] A. Richter, Prog. Part. Nucl. Phys. **34** (1995) 261.

[33] K. Langanke, G. Martínez-Pinedo, Nucl. Phys. A **673** (2000) 481.